



1 **Quantification of hydraulic trait control on plant hydrodynamics and risk of hydraulic**
2 **failure within a demographic structured vegetation model in a tropical forest (FATES-**
3 **HYDRO V1.0)**

4 Chonggang Xu¹, Bradley Christoffersen², Zachary Robbins¹, Ryan Knox³, Rosie A. Fisher⁴,
5 Rutuja Chitra-Tarak¹, Martijn Slot⁵, Kurt Solander¹, Lara Kueppers^{3,6}, Charles Koven³, Nate
6 McDowell^{7,8}

7 1: Earth and Environmental Sciences Division, Los Alamos National Laboratory, Los Alamos
8 NM, USA

9 2: Biology Department, University of Texas Rio Grande Valley, TA, USA

10 3: Lawrence Berkeley National Laboratory, Berkeley, CA USA

11 4: CICERO Centre for International Climate Research, Oslo, Norway

12 5: Smithsonian Tropical Research Institute, Apartado 0843-03092, Balboa, Ancon, Republic of
13 Panama

14 6: Energy and Resources Group, University of California, Berkeley, CA USA

15 7: Atmospheric Sciences and Global Change Division, Pacific Northwest National Laboratory,
16 Richland, WA, USA

17 8: School of Biological Sciences, Washington State University, Pullman, WA, USA

18

19

20

21

22 Corresponding author: Chonggang Xu (cxu@lanl.gov)

23



24 **Abstract:** Vegetation plays a key role in the global carbon cycle and thus is an important
25 component within Earth system models (ESMs) that project future climate. Many ESMs are
26 adopting methods to trace the size and succession-stage-structure of plants within demographic
27 models. These models make it feasible to conduct more realistic simulation of processes that
28 control vegetation dynamics. Separately, increasing understanding of the ecophysiological
29 processes governing plant water use, and the need to understand ecosystem responses to drought
30 in particular, has led to the adoption of physical plant hydrodynamic schemes within ESMs. In this
31 study, we report on a new hydrodynamics (HYDRO) model incorporated in the Functionally
32 Assembled Terrestrial Ecosystem simulator (FATES). The size and canopy structured
33 representation within FATES is able to simulate how plant size and hydraulic traits affect
34 vegetation dynamics and carbon/water fluxes. To better understand this new model system and its
35 functionality in tropical forest systems in particular, we conducted a global parameter sensitivity
36 analysis at Barro Colorado Island, Panama. We assembled observations of plant hydraulic traits
37 for stomata, leaves, stems, and roots, and determined the best-fit statistical distribution for each
38 trait. Our model analysis showed that the taper component determining hydraulic conductivity
39 tapering from trunk to branch, the water potential leading to 50% loss (P_{50}) of stomatal
40 conductance, the maximum hydraulic conductivity for the stem, and the fraction of total hydraulic
41 resistance in the above ground section are the top 5 traits determining the simulated water potential
42 and loss of conductivity for different plant organs. For the risk of hydraulic failure and potential
43 tree mortality, we found that ensemble members with high risk of mortality generally have a higher
44 taper exponent and a higher xylem conductivity, less negative P_{50} for stomata conductance, and
45 more negative P_{50} for stem and transporting roots. We expect that our results will provide guidance
46 on future modeling studies using plant hydrodynamic models to predict the forest responses to



47 droughts, and future field campaigns that aim to better parameterize the plant hydrodynamic

48 model.

49



50

51 **1. Introduction**

52 Tropical forests play a critical role in regulating regional and global climates (Bonan,
53 2008). Under ongoing and future climate change, they are subjected to substantial risks of
54 climate extremes such as drought and heat waves (Mcdowell et al., 2018). Studies have already
55 shown that tropical forests were experiencing elevated tree mortality rates due to mega
56 droughts related to ENSO events. For example, the 2015–16 El Niño led to the death of an
57 estimated 2.5 ± 0.3 billion stems in the Lower Tapajós river basin of the Amazon and the
58 associated carbon loss had not yet been compensated by new plant growth three years after the
59 event (Berenguer et al., 2021). Such extreme climate events are projected to increase in
60 frequency and intensity under a warming future. A statistical analysis based on the projection
61 of 13 ESMs under a high greenhouse emission scenario showed that the frequency of extreme
62 droughts as defined by rhizosphere soil moisture (occurring once every 50 years) could
63 increase by a factor of nearly 4 and this increase would have substantially more impact on
64 tropical forests (Xu et al., 2019). The high species diversity found in tropical forests may result
65 in increased resilience to climate extremes, based on the demonstrated resilience of temperate
66 forests in relationship to trait diversity (Anderegg et al., 2018). However, due to limited data
67 to parametrize and constrain models for tropical forests, there is a large uncertainty in our
68 predictive understanding of how tropical forests will respond to these climate extremes (Bonal
69 et al., 2016). This uncertainty is considered to be a key source of uncertainty in our projection
70 of land carbon fluxes and future climates (Arora et al., 2020).

71 Earth System Models (ESMs) have been developed to project future changes to the coupled
72 climate and biosphere system. Typically, ‘big leaf’ approximations of vegetation with no



73 explicit presentation of tree size and canopy structure have been used to predict the impact of
74 vegetation on carbon and water cycles. These models do not represent the fundamental
75 elements of vegetation dynamics including mortality, competition, and growth, and their
76 response to disturbances. In the last decade, many ESMs have incorporated vegetation
77 demographic models (VDMs) that represent plant size, canopy structure and disturbance
78 histories, with the goal of better representing the competitive dynamics among different size
79 classes of trees and plant functional types in response to climate and vegetation disturbance
80 (Fisher et al., 2018). Most of these VDMs can differentiate plants' light, water and carbon use
81 strategies and can thus represent some part of the functional diversity of tropical forests
82 (Massoud et al., 2019; Koven et al., 2020).

83 Following the 'big leaf' model, water limitation on plant gas exchange in these VDMs is
84 generally calculated based on three factors: 1) soil water potential; 2) root distribution; and 3)
85 water potential for stomata openness and closure, all of which differ by plant functional type
86 (Koven et al., 2020). While such water limitation functions are able to capture trait diversity
87 in leaf-level stomatal behaviors, they fail to capture plant functional diversity in many other
88 observable plant hydraulic traits, such as xylem capacitance, water potentials for loss of xylem
89 hydraulic conductivity, stem hydraulic safety margin, and turgor loss point (Hochberg et al.,
90 2018). Many studies have shown that plant hydraulic traits play an important role in plant
91 responses to droughts (Su et al., 2022; Anderegg et al., 2016), which could shape the landscape
92 distribution of plant functional types (Kunert et al., 2021). In view of this limitation, plant
93 hydrodynamic models have been developed with the aim of better simulating forest response
94 to droughts (Powell et al., 2018; Christoffersen et al., 2016; Xu et al., 2016; Kennedy et al.,
95 2019). These models not only allows us to better incorporate hydraulic functional diversity,



96 but also allow us to mechanistically simulate the risk of plant mortality due to hydraulic
97 functional failure resulting from embolism in xylem.

98 One key challenge for these plant hydrodynamic models is that they have many more
99 parameters than simple water limitation functions based on soil water potentials and thus
100 inherently possess more uncertainty in the model parameterization and subsequent simulations.
101 In this study, we describe the implementation of a hydrodynamic scheme within FATES, and
102 assess this new configuration with two goals: 1) assess the importance of different hydraulic
103 traits in determining plant hydrodynamics; and 2) identify key hydraulic traits that are
104 important for predicting the risk of mortality due to hydraulic failure. We expect that our results
105 will provide guidance on model parameterization for future modeling studies using plant
106 hydrodynamic models to predict tropical forest response to droughts, and future field
107 campaigns that aim to collect observational data that can be used to better parameterize and
108 benchmark plant hydrodynamic models.

109 **2. Methodology**

110 **2.1. Model description**

111 We use the functionally assembled terrestrial ecosystem simulator (FATES), a VDM that
112 is coupled within the Energy Exascale Earth System Model (E3SM) (Caldwell et al., 2019).
113 FATES represents size-structured groups of plants (cohorts) and successional trajectory-based
114 patches using the ecosystem demography approach (Fisher et al., 2015; Moorcroft et al., 2001).
115 FATES simulates growth by integrating photosynthesis across different leaf layers for each
116 cohort. FATES allocates this photosynthate to different tissues including leaves, fine and
117 coarse roots, and stem, based on the allometry of different plant functional types, as well as a
118 carbon storage pool (Fisher et al., 2015). Mortality within FATES is simulated by several



119 mechanisms, including carbon starvation caused by depletion of the storage pool, hydraulic
120 function failure, as well as impact mortality during disturbance, fire, logging, freezing, age-
121 related and ‘background’ constant turnover (Fisher et al., 2015; Huang et al., 2020; Fisher et
122 al., 2010; Needham et al., 2020).

123 The default model contains a simplistic algorithm that approximates plant hydraulic failure
124 thresholds based on soil water potential. An important feature of the plant hydrodynamic
125 scheme (HYDRO), which explicitly simulates water flow from the soil through leaves to the
126 atmosphere, is that it enables direct representation of percent loss conductance as a predictor
127 of hydraulic failure mortality rates. FATES-HYDRO is based on the hydrodynamic model
128 implemented in the Traits-based Forest Simulator (TFS) (Christoffersen et al., 2016). The
129 water flow is calculated based on water pressure gradients across different plant compartments
130 (rhizosphere, absorbing roots, transporting roots, stem, and leaf). Specifically, flow between
131 compartment i and $i + 1$ (Q_i) is given by

$$Q_i = -K_i \Delta h_i, \quad (1)$$

132 where K_i is the total conductance ($\text{kg MPa}^{-1} \text{s}^{-1}$) at the boundary of compartments i and $i + 1$
133 and Δh_i is the total matric potential difference between the compartments:

$$\Delta h_i = \rho_w g (z_i - z_{i+1}) + (\psi_i - \psi_{i+1}), \quad (2)$$

134 where z_i is compartment elevation difference above (+) or below (-) the soil surface (m), ρ_w
135 is the density of water (10^3 kg m^{-3}), g is acceleration due to gravity (9.8 m s^{-2}), and ψ_i is tissue
136 or soil matric water potential (MPa). K_i is treated here as the product of a maximum boundary
137 conductance between compartments i and $i + 1$ ($K_{max,i}$), and the fractional maximum
138 hydraulic conductance of the upstream compartments (FMC_i or FMC_{i+1}), which is a function
139 of the tissue water content.



140 The plant hydrodynamic representation and numerical solver scheme within FATES-
141 HYDRO follows the 1-D solver laid out by Christoffersen et al. (2016). The equations are
142 solved for tissue water content at a 30 minutes time step. We made a few modifications to
143 accommodate the multiple-soil layers and improve the numerical stability. First, to
144 accommodate the multiple-soil layers, we sequentially solve the Richards' equation for each
145 individual soil layer, with each layer-specific solution proportional to each layer's contribution
146 to the total root-soil conductance. Second, to improve the numerical stability, we now linearly
147 interpolate the pressure/volume curve beyond the residual and saturated tissue water content
148 to avoid the rare cases of overshooting in the numerical scheme under very dry or wet
149 conditions. Please see the Supplementary Information [HYDRO_DESCRIPTION.pdf] for
150 details of the implementation.

151 In this study, as our focus is on the plant hydrodynamics, we used the static stand structure
152 mode of FATES that turns off the processes of competition, growth and mortality, to instead
153 hold the ecosystem structure constant. This reduced-complexity configuration (Fisher and
154 Koven, 2020) thus exercises only the primarily fast-timescale-processes of photosynthesis,
155 transpiration, water transport, and plant hydrodynamics (i.e., change in hydraulic conductivity,
156 water storage, and water potentials in plant tissues). By using static stand structure mode, as in
157 Chitra-Tarak et al. (2021), we isolate hydraulic trait controls on simulated hydrodynamics and
158 avoid confounding, and potentially biased, feedbacks from resulting changes in forest
159 structure. The forest stand structure include tree size and composition is initialized based on
160 the forest inventory data in 2017. As the majority of species in BCI is evergreen broad leaf
161 trees, we run the model with one PFT with different hydraulic traits (Table 1) to assess their
162 impact on the hydrodynamically relevant outputs including water potentials and fraction of



163 maximum conductivity for different plant organs including absorbing root, transporting root,
164 stem, and leaves and risk of hydraulic failure. FATES simulates the carbon and water fluxes
165 for different size classes of trees. Because large trees experience more fluctuation in
166 environmental conditions in the canopy, here we focused on hydrodynamic behaviors for trees
167 of diameter more than 60 cm.

168 **2.2. Parametric uncertainty estimation**

169 We identified 36 parameters for the FATES-HYDRO model (Table 1). To estimate the
170 parameter distributions, we started with published meta-analyses (Christoffersen et al., 2016;
171 Choat et al., 2012; Bartlett et al., 2012; Bartlett et al., 2014; Bartlett et al., 2016; Klein, 2014)
172 and supplemented them with select new data from individual studies. Focal data were tissue-
173 or individual-level hydraulic traits spanning water transport and embolism resistance, tissue
174 water storage and retention (PV curve traits), hydraulic architecture (i.e., leaf area to sapwood
175 area ratio), stomatal responses to dehydration, and fine root traits (Table 1). For each dataset,
176 we standardized taxonomic names using the TNRS package in R (Boyle et al., 2013). This
177 allowed us to join datasets together based on species, averaging multiple observations per
178 species if necessary, resulting in a species-specific sparse matrix of all hydraulic traits for all
179 databases and individual studies that we compiled. This pantropical hydraulic trait dataset is
180 included in the Supporting Information [traits_master_trop.csv].

181 We then determined parametric distributions which best fit the trait data. Where necessary,
182 traits were transformed to be positive, and certain traits with well-defined upper and lower
183 bounds were normalized on [0, 1] according to $(x - x.lowerbound)/(x.upperbound -$
184 $x.lowerbound)$ for trait x (Table 1). For each trait, we used parameter estimates for the
185 distribution with the largest log likelihood among all possible distributions using fitdistr



186 package in R. We augmented observations with extratropical data to increase sample size for
187 traits with less than three tropics-specific observations. Where trait data were mostly
188 unmeasured, we used a uniform distribution bounded on our best estimate of the theoretical
189 range (Table 1). As there is limited data on roots, we used the same distribution as that for
190 branches if data was missing. Because our goal is to understand the model behaviors as
191 determined by different hydraulic traits, we assumed independence among traits. As we
192 focused on the hydraulic traits in this study, we used non-hydraulic trait values based on an
193 optimal set of parameters that best fit observed water and carbon fluxes in FATES
194 implemented without hydrodynamics (Koven et al., 2020).

195 **2.3. Sensitivity analysis**

196 We used the Fourier Amplitude Sensitivity Test (FAST) to assess the relative importance
197 of parameters in determining the variance of model outputs (Xu and Gertner, 2011a). The main
198 idea of FAST is to assign periodic signals in the sampled parameter values and use Fourier
199 transformation to identify the signals in the outputs. Sampled parameter values are based on
200 Latin hypercube sampling from the fitted statistical distributions (see previous section for more
201 details). We ran 1000 ensemble simulations of the FATES-Hydro to derive model outputs of
202 water potential and fraction of maximum conductivity. We used the Uncertainty Analysis and
203 Sensitivity Analysis (UASA) tool (<https://sites.google.com/site/xuchongang/uasatoolbox>) to
204 estimate the parameter importance, which is defined as the proportion of total model output
205 variance contributed by individual model parameters. For details, please refer to Xu and
206 Gertner (2011a). We run the model with 1000 ensemble members, in view that an order of 100
207 times effective important number of parameters, which we estimate to be ~10, is needed to
208 achieve reasonable precision (Xu and Gertner, 2011b).



209 **2.4. Study area and climate drivers**

210 In this study, we used Barro Colorado Island (BCI), Panama, as our test site to evaluate
211 model behavior. We chose BCI as it has moderately strong dry and wet seasons that allow us
212 to assess the hydrodynamics under different levels of water availability. Moreover, extensive
213 field campaigns in recent years have provided comprehensive data needed for model
214 parameterization, initialization and climate drivers. Finally, we also leverage prior FATES
215 studies of non-hydraulic parameters at BCI (Koven et al., 2020).

216 BCI has an annual mean temperature of 26.3°C and an annual mean precipitation of 2656
217 mm with a strong seasonal precipitation signal. The dry season lasts from January to April,
218 with a mean precipitation of 228mm, while the wet season lasts from May-December with a
219 mean precipitation of 2428mm (Paton, 2020). In this study, we used hourly in-situ climate data
220 from 2008-2016 to drive the model. To run the model to equilibrium (in terms of soil moisture
221 content) takes 5-6 years, thus we choose February of 2016 as the target for analysis of dry
222 season hydrodynamics and August of 2016 as the target for analysis of wet season
223 hydrodynamics. Using static stand structure mode means that we do not need to spin up
224 vegetation state and thus reducing the simulation time.

225 **3. Results**

226 Our results showed that the simulated ranges across the ensemble of leaf water potential
227 (Fig. 1) and loss of conductivity (Fig. 2) are large. For leaf water potential, the 95% percentile
228 ranges are from -5 MPa to -0.5 MPa and -3 MPa to -0.5 Mpa for February and August 2016,
229 respectively. Correspondingly, the fraction of maximum stem hydraulic conductivity is much
230 higher during August compared to February (Fig. 2); however, in both months, the modeled
231 range spans almost the full range of between 0 and 1.



232 Based on the FAST sensitivity indices (i.e., the variance in model output contributed by
233 different parameters), the key parameters that control the water potentials of different plant
234 organs (leaf, stem and root) include the taper exponent for hydraulic conductivity (p_taper),
235 the water potential leading to 50% loss of stomatal conductance ($p50_gs$), maximum hydraulic
236 conductivity for the stem ($kmax_node_stem$), and the fraction of total hydraulic resistance in
237 the above ground section ($rfrac_stem$), in decreasing order (Fig. 3). For the fractional loss of
238 conductivity, the most important parameter is the water potential leading to 50% loss of
239 hydraulic conductance (P_{50}) for the corresponding organs (Fig. 4). Other important parameters
240 are similar to those for simulated water potentials. Notably, the organ-specific P_{50} values are
241 more important for the dry month (February) compared to the wet month (August). For the wet
242 month of August, p_taper is the dominant parameter controlling the pre-dawn and midday loss
243 of hydraulic conductivity, while organ-specific P_{50} parameters are the second most important.

244 In terms of the risk of hydraulic failure, out of the 1000 ensemble members, 40-60% of the
245 simulations suggest that branches are the most vulnerable plant organ, based on highest loss of
246 conductivity across the continuum from root to branch (Fig. 5). For the dry month of February,
247 roots are at greater risk in comparison to the wet season. If we consider the loss of conductivity
248 more than 50% for February 2016 as a threshold for a high risk of mortality (Adams et al.,
249 2017), then 53% of ensemble simulations reach this threshold. The key parameters affecting
250 the risk of mortality, as measured by percentage difference in parameter values for ensemble
251 members reaching 50% loss of conductivity or not, include the water potential leading to 50%
252 loss of conductance for stomata ($p50_gs$), stem ($p50_node_stem$), and transporting roots
253 ($p50_node_root$), maximum hydraulic conductivity of stem ($kmax_node_stem$), and the taper
254 exponent (p_taper) (Fig. 6). Ensemble members with high risk of mortality generally have a



255 higher p_taper and $kmax_node_stem$, less negative $p50_gs$, and more negative $p50$ for stem
256 and transporting roots (Fig. 7).

257 4. Discussion

258 Our analysis showed the importance of key plant hydraulic traits in simulating plant water
259 potential and risk of hydraulic failure. This analysis identifies these parameters as potential
260 targets of either model calibration or targeted measurement campaigns to achieve realistic
261 simulations. In our sensitivity analysis, the most influential parameter for both water potential
262 and loss of conductivity is the tapering of the radius of conduit with increasing plant height
263 (p_taper). As p_taper increases, the conduit radius increases from the top of the tree to its base.
264 According to Hagen-Poiseuille's equation, this increases the theoretical maximum total
265 conductance. Low values of p_taper thus limit the adverse effects of tree height by increasing
266 k_max along the whole continuum and reducing the soil-to-leaf water potential needed to
267 maintain transpiration. Our inference is that p_taper represents an overarching property of
268 plant architecture that influences the relative effect of each of the other parameters with regard
269 to hydraulic safety and efficiency. While p_taper is less directly related to plant adaptations to
270 drought, the architecture of the plant itself determines the range of values that give rise to
271 drought adaptive strategies. Another dimension of the hydraulic architecture with a critical role
272 in determining both water potential and loss of conductivity, though to a much lesser degree,
273 was the fraction of total tree resistance within the above-ground stem ($rfrac_stem$). Generally,
274 a plant will maintain this resistance, matching the growth of trunk and crown height to maintain
275 total resistance as the distance water needs to travel increases (Yang and Tyree, 1993). In this
276 study, due to the lack of data on the belowground resistance, we assigned a quite large range



277 for this trait, which could be impact by many factors such as belowground root biomass and
278 interaction between root, fungi and bacteria.

279 The second most sensitive parameter in determining loss of conductance was the leaf water
280 potential at 50% loss of stomatal conductance (*p50_gs*). The parameter controls the water loss
281 rate from leaf and a less negative value provides protection from hydraulic failure during water
282 limited periods. It has been shown to play a key role in tree survival during severe droughts
283 (Breshears et al., 2009; Rowland et al., 2015). The ability to withstand lower leaf water
284 potentials is also a key indicator of sapling and seedling survival during drought and
285 determines species distribution across a moisture gradient (Kursar et al., 2009). There may be
286 a trade-off between drought tolerance (with a lower *p50_gs*) and drought avoidance (a less
287 negative *p50_gs* but with a high capacitance; the amount of water released from reserves as
288 leaf water potential declines), a crucial aspect in determining species drought resistance
289 (Pineda-Garcia et al., 2013). Additionally, loss of conductivity was sensitive to the water
290 potential at 50% loss of max conductivity within the stem (*p50_stem*) as it can largely affect
291 the whole plant conductance and thus the water supply to the leaves. *p50_stem* negatively
292 correlates with wood density and may be a marker of the trade-off between hydraulic efficiency
293 and safety within the stem (Chen et al., 2009; Manzoni et al., 2013). Even though we did not
294 consider this trade-off as we mainly focused on the hydraulic traits in this study, this trade-off
295 could be important to consider for competitions and co-existence among different plant
296 functional types.

297 Leaf water potential and loss of conductance were both sensitive to the maximum xylem
298 conductivity in the stem (*kmax_node_stem*). Higher maximum conductivity represents greater
299 xylem efficiency, which in the absence of drought or light limitations would result in greater



300 potential photosynthesis and less negative water potentials (Gleason et al., 2016). However,
301 xylem with higher $k_{max_node_stem}$ could be more vulnerable to embolism as water potential
302 declines (Sperry and Love, 2015). In tropical rainforests, species with higher conductivity per
303 unit leaf area generally are less desiccation tolerant and exhibit higher mortality rates (Kursar
304 et al., 2009). Low $k_{max_node_stem}$ along with high leaf-to-sapwood area ratio ($la2sa$) also
305 represents a vulnerability to reduced conductance which increases with height (Christoffersen
306 et al., 2016).

307 Traits with lower order of impacts on water potential modulate the amount of stored water
308 available during drought. The fraction of water in the capillary reserve within the stem (f_{cap})
309 determines the amount of water stored within the stem. Water storage in the stem has been
310 shown to help maintain higher water potentials as drought continues (Bartlett et al., 2019). The
311 bulk modulus of elasticity in the root ($epsil_node$) determines the amount of water available
312 from cellular storage between complete hydration and loss of turgor (Powell et al., 2017). This
313 represents the ability of the roots to continually supply water to the rest of the plant as drought
314 occurs. It also represents an investment in cellular structure, which may be an additional
315 indicator of adaptations with non-hydraulic origin.

316 The sensitivity of vegetation to drought stress and hydraulic failure induced mortality is
317 of paramount importance for understanding how ecosystems may respond to shifting
318 temperature and rainfall patterns under a changing climate (Mcdowell et al., 2022). We
319 recognize that parametric sensitivity could be different for different sites depending on climate
320 driver, soil moisture and vegetation types. However, we expect the main parameter of
321 importance could be could be useful to guide model calibration to select the candidate
322 parameters for different sites. As understanding of plant hydrodynamics increases, linking



323 model predictions to observable plant traits has emerged as a promising means of constraining
324 predictions of ecosystem resilience. Such traits are challenging and costly to measure in the
325 field and thus resources must be directed carefully when planning measurement campaigns.
326 The identified parameters in this study could provide guidance on the limited measurement we
327 could target in the field.

328 **5. Acknowledgment**

329 This research was supported as part of the Next Generation Ecosystem Experiments-
330 Tropics, funded by the U.S. Department of Energy, Office of Science, Office of Biological and
331 Environmental Research.

332 **6. CODE and Data Availability**

333 The FATES-HYDRO code is available from <https://doi.org/10.5281/zenodo.7686333>. The
334 traits data are in the supplementary file [traits_master_trop.csv].

335 **7. Supplement Information**

336 Two supplementary file are included. The HYDRO_DESCRIPTION.pdf provide the
337 summary of the hydrodynamic implementation that is different from Christoffersen et al.
338 (2016). The traits_master_trop.csv file include all the hydraulic traits we assembled for the
339 tropical region.

340 **8. Author contribution**

341 CX and BC designed the sensitivity analysis experiments. BC collected the data and fitted
342 the trait distributions. CX conducted the analysis and drafted the manuscript. BC, CX, RF, RN
343 and CK designed the implementation of HDRO codes. BC implemented the majority of
344 HDRO codes with code improvement made by CX and RN. ZR conducted the ensemble model
345 simulations. MS provided the leaf cuticular conductance data. NM, CK and LK provided



346 guidance on the sensitivity analysis, code development and trait data synthesis. All authors
347 contributed to manuscript writing by providing edits and suggestions.

348 **9. Competing interests**

349 The contact author has declared that none of the authors has any competing interests.

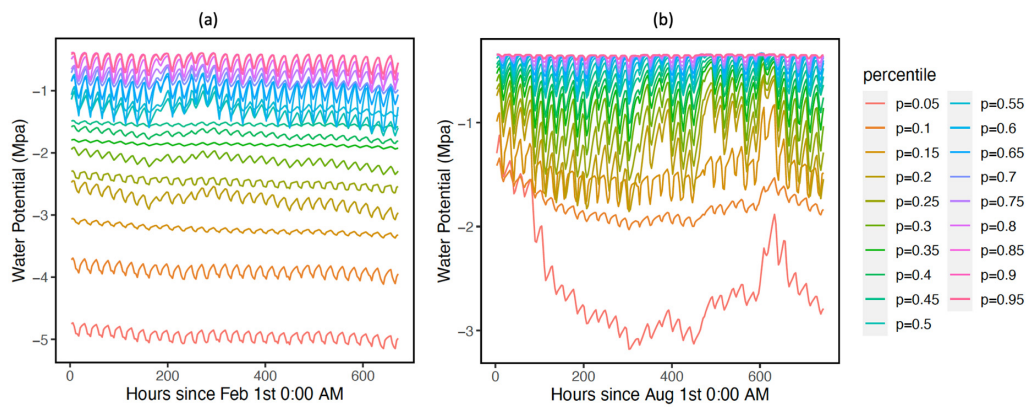
350



351

352 **Figures**

353



354

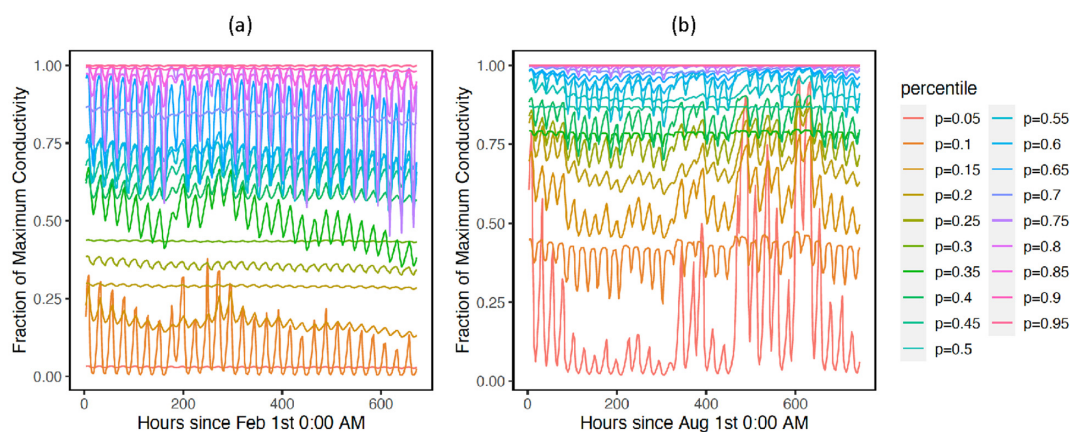
355

356 **Figure 1: Simulated ranges of leaf water potential for February (a) and August (a), 2016.** The percentiles are calculated
357 based on the monthly mean values of leaf water potentials for the 1000 ensemble simulations.

358



359



360

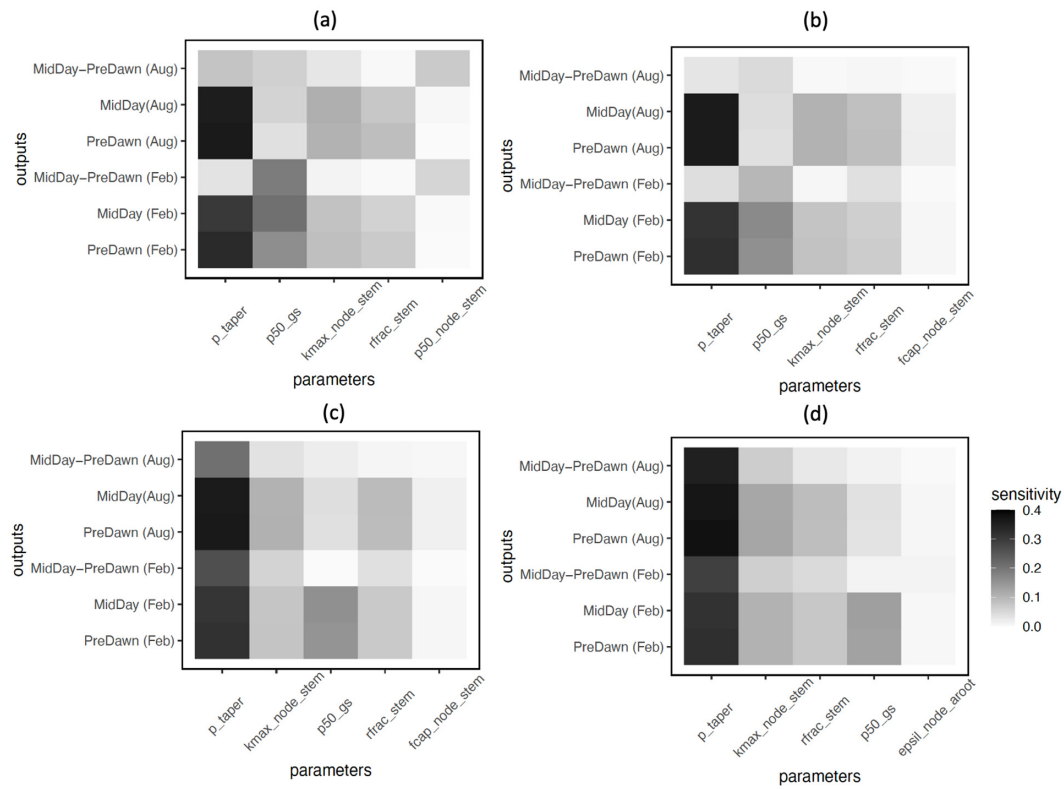
361 **Figure 2: Simulated ranges of fraction of maximum hydraulic conductivity of stem for February (a) and August (a),**

362 **2016. The percentiles are calculated based on the monthly mean values of leaf water potentials for the 1000 ensemble**

363 **simulations.**

364

365



366
367

Figure 3: Key parameters that control simulated water potentials for leaf (a), stem (b), transporting root (c) and

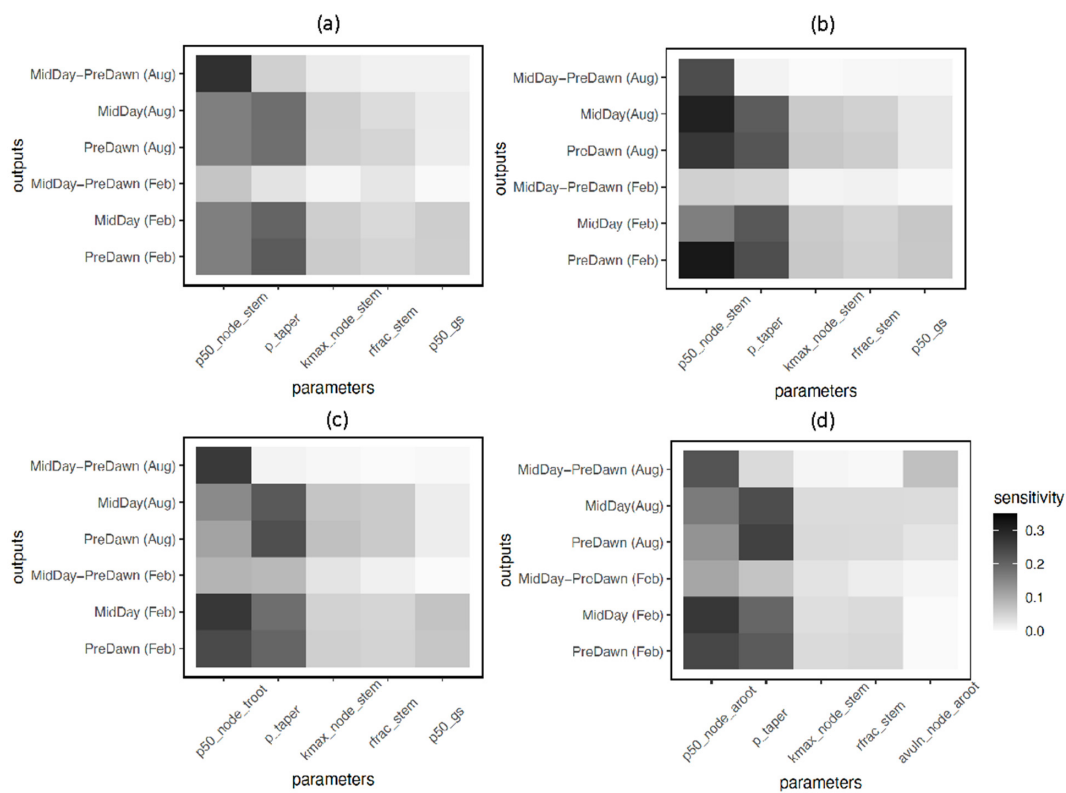
368

absorbing root (d). The sensitivity value refers to the proportion of total model output variance contributed by a specific

369

parameter (0-1). See Table 1 for the explanation of the parameters.

370



371

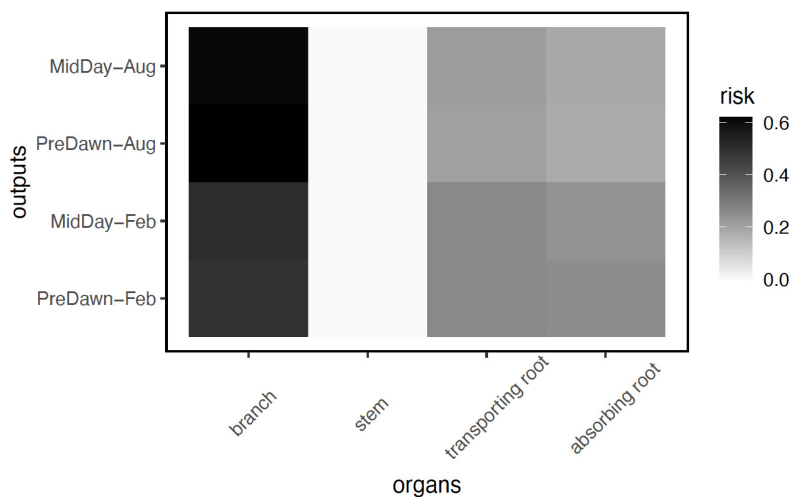
372

373 **Figure 4: Key parameters that control simulated loss of conductivity for branch (a), stem (b), transporting root (c) and**

374 **absorbing root (d).** The sensitivity value refers to the proportion of total model output variance contributed by a specific

375 parameter. See Table 1 for the explanation of the parameters. See Table 1 for the description of parameters.

376



377

378 **Figure 5: Risk on the continuum for hydraulic failure as measured by percentage of total number of simulations with**
379 **highest loss of conductivity for a specific organ (branch, stem, transporting root and absorbing root).** As the model does
380 not specifically simulate the branch, we calculated the risk of loss of conductivity based on the leaf water potential and hydraulic
381 vulnerability curve from xylem.

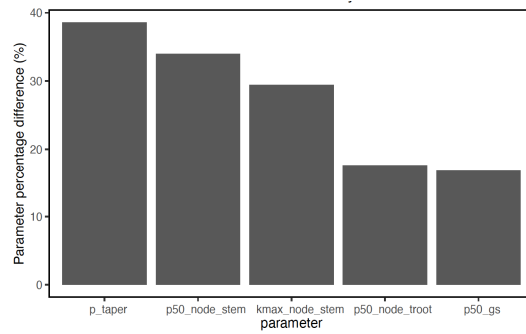
382



383

384

385

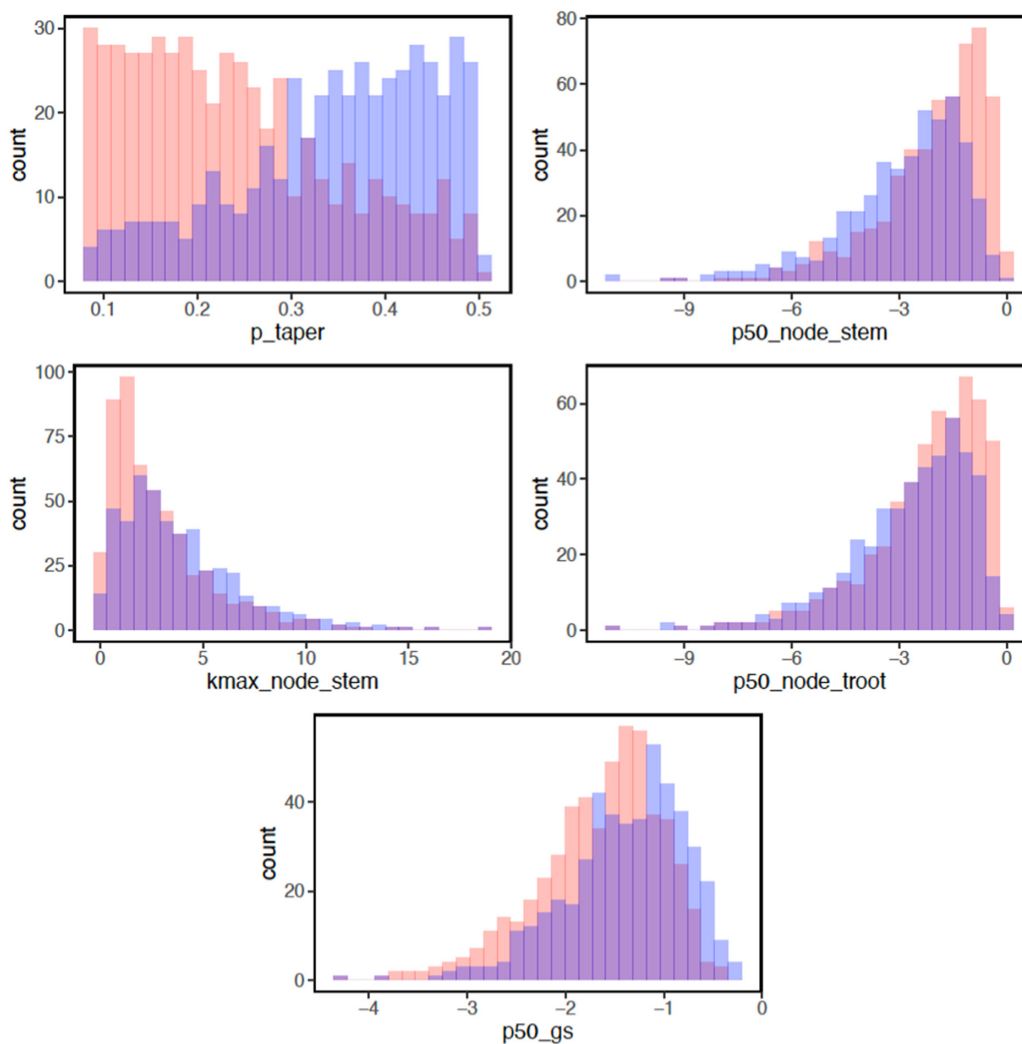


386

387 **Figure 6: Mean trait percentage difference for model ensemble simulations with loss of hydraulic conductivity larger**
388 **than 50% and ensemble simulations with loss of hydraulic conductivity less than 50%. See Table 1 for the description of**
389 parameters.

390

391



392

393 **Figure 7: Parameter difference for ensemble members with risk of mortality.** Blue bars indicate parameter values with
394 lower mortality risk (<50% loss of hydraulic conductivity). Red bars indicate parameter values with higher mortality risk (\geq
395 50% loss of hydraulic conductivity) and purple bars indicate parameter values stacked from transparent red/blue bars. See Table
396 1 for the description of parameters.

397

398



399

400 Table 1 Hydraulic parameters considered in the sensitivity analysis

PARAMETER	SYMBOL	UNITS	DISTRIBUTION ¹	SOURCES& NOTES
Pressure-Volume (PV) curve (water content – water potential relationship)				
saturated water content (thetas_node)	θ_s	cm ³ cm ⁻³	Leaf: Beta (9.69, 6.20) Stem: Beta (12.67, 7.4626) TRoot and AROOT: Beta (22.98, 5.29)	Christoffersen et al. (2016) Iversen et al. (2017) Wright et al. (2010) Roderick et al. (1999) Sack et al. (2003) Binks et al. (2016)
turgor loss point (tlp_node)	π_{tlp}	MPa	-	Bartlett et al. (2012); $\pi_{tlp} = (\pi_0 \epsilon) / (\pi_0 + \epsilon)$
osmotic potential at full turgor (pinot_node)	π_0	MPa	Leaf: G [9.8,6.26], Stem, TRoot, ARoot: LN [0.32,0.39]	Bartlett et al. (2012, 2014, 2016) and Christoffersen et al. (2016)
bulk elastic modulus (epsil_node)	ϵ	MPa	Leaf: G (4.07, 4.12) Stem, TRoot and ARoot: G [3.57, 3.84]	Bartlett et al. (2012, 2014), and Christoffersen et al. (2016)
residual water fraction(resid_node)	RWC_r	unitless	Leaf: B [2.14,4.10] Stem, TRoot and ARoot: B [2.71, 4.53]	Bartlett et al. (2012, 2014), Christoffersen et al. (2016)
fraction of water in capillary reserve (fcap_node)	f_{cap}	unitless	U [0.1, 0.7]	Christoffersen et al. (2016)
Vulnerability Curve (water potential – hydraulic conductivity relationship)				
water potential at 50% loss of max conductivity (p50_node)	$P_{50,x}$	MPa	Stem, TRoot and ARoot: G [2.07, 1.18]	Choat et al. (2012)
vulnerability curve shape parameter (avuln_node)	a_x	unitless	Stem, TRoot and ARoot: LN [0.82,0.66]	Choat et al. (2012)



xylem conductivity per unit sapwood area (<i>kmax_node_stem</i>)	$k_{s,max}$	kg m ⁻¹ s ⁻¹ MPa ⁻¹	G [1.41, 2.37]	Choat et al. (2012)
Leaf hydraulics				
leaf water potential at 50% loss of max gs (<i>p50_gs</i>)	$P_{50,gs}$	MPa	G [5.73, 0.27]	Klein (2014)
stomatal vulnerability shape parameter(<i>avuln_gs</i>)	a_{gs}	unitless	-	Christoffersen et al. (2016); derived according to empirical equation: $a_{gs} = -2.406 P_{50,gs}$ ($-P_{50,gs}$) ^{-1.25}
Leaf cuticular conductivity (<i>k0_leaf</i>)	$k_{0,l}$	umol m ⁻² s ⁻¹	LN [1.04,0.84]	This study, based on data measured by Martijn Slot
Plant Hydraulic Architecture				
Xylem taper exponent for sapwood (<i>p_taper</i>)	p	(-)	U (0.08, 0.5)	Savage et al. (2010)
Leaf area to sapwood area ratio (<i>la2sa</i>)	<i>la2sa</i>	(-)	LN (-0.48, 0.77)	Choat et al. (2012)
Root hydraulic Traits				
specific root length (<i>srl</i>)	<i>srl</i>	m g ⁻¹	G [1.70, 35.31]	Iversen et al. (2017)
absorbing root radius (<i>rs2</i>)	r	mm	LN [-1.91, 0.79]	Iversen et al. (2017)
fraction of total tree resistance that is aboveground (<i>rfrac_stem</i>)	<i>rfrac</i>	Unitless	U [0.1,0.7]	This study; empirical
root-soil interface conductivity per unit surface area (<i>Kr1</i>)	$k_{r1,max}$	kg m ⁻¹ s ⁻¹ MPa ⁻¹	G [1.41, 2.37]	This study; empirically set the same as xylem conductivity
maximum root water loss rate (<i>Kr2</i>)	$k_{r2,max}$	kg m ⁻¹ s ⁻¹ MPa ⁻¹	LN [-6.80, 0.92]	Wolfe (2020); Empirically set as 1/1000 bark water loss rate

401 **Note:** 1:B-Beta distribution; U- Uniform distribution [lower limit, upper limit]; N-Gaussian
 402 distribution (mean, standard deviation); LN-Log Normal Distribution [mean, standard deviation];
 403 G-Gamma distribution (lambda, scale); TRoot-Transporting root; ARoot-Absorbing root.

404



405 Reference

- 406 1. Adams, H. D., Zeppel, M. J. B., Anderegg, W. R. L., Hartmann, H., Landhausser, S. M.,
407 Tissue, D. T., Huxman, T. E., Hudson, P. J., Franz, T. E., Allen, C. D., Anderegg, L. D.
408 L., Barron-Gafford, G. A., Beerling, D. J., Breshears, D. D., Brodrigg, T. J., Bugmann,
409 H., Cobb, R. C., Collins, A. D., Dickman, L. T., Duan, H. L., Ewers, B. E., Galiano, L.,
410 Galvez, D. A., Garcia-Forner, N., Gaylord, M. L., Germino, M. J., Gessler, A., Hacke, U.
411 G., Hakamada, R., Hector, A., Jenkins, M. W., Kane, J. M., Kolb, T. E., Law, D. J.,
412 Lewis, J. D., Limousin, J. M., Love, D. M., Macalady, A. K., Martinez-Vilalta, J.,
413 Mencuccini, M., Mitchell, P. J., Muss, J. D., O'Brien, M. J., O'Grady, A. P., Pangle, R.
414 E., Pinkard, E. A., Piper, F. I., Plaut, J. A., Pockman, W. T., Quirk, J., Reinhardt, K.,
415 Ripullone, F., Ryan, M. G., Sala, A., Sevanto, S., Sperry, J. S., Vargas, R., Vennetier, M.,
416 Way, D. A., Xu, C. G., Yezpez, E. A., and McDowell, N. G.: A multi-species synthesis of
417 physiological mechanisms in drought-induced tree mortality, *Nat Ecol Evol*, 1, 1285-
418 1291, 10.1038/s41559-017-0248-x, 2017.
- 419 2. Anderegg, W. R. L., Klein, T., Bartlett, M., Sack, L., Pellegrini, A. F. A., Choat, B., and
420 Jansen, S.: Meta-analysis reveals that hydraulic traits explain cross-species patterns of
421 drought-induced tree mortality across the globe, *P Natl Acad Sci USA*, 113, 5024-5029,
422 10.1073/pnas.1525678113, 2016.
- 423 3. Anderegg, W. R. L., Konings, A. G., Trugman, A. T., Yu, K. L., Bowling, D. R.,
424 Gabbitas, R., Karp, D. S., Pacala, S., Sperry, J. S., Sulman, B. N., and Zenes, N.:
425 Hydraulic diversity of forests regulates ecosystem resilience during drought, *Nature*, 561,
426 538–541, 10.1038/s41586-018-0539-7, 2018.
- 427 4. Arora, V. K., Katavouta, A., Williams, R. G., Jones, C. D., Brovkin, V., Friedlingstein,
428 P., Schwinger, J., Bopp, L., Boucher, O., Cadule, P., Chamberlain, M. A., Christian, J. R.,
429 Delire, C., Fisher, R. A., Hajima, T., Ilyina, T., Joetzjer, E., Kawamiya, M., Koven, C.
430 D., Krasting, J. P., Law, R. M., Lawrence, D. M., Lenton, A., Lindsay, K., Pongratz, J.,
431 Raddatz, T., Seferian, R., Tachiiri, K., Tjiputra, J. F., Wiltshire, A., Wu, T. W., and
432 Ziehn, T.: Carbon-concentration and carbon-climate feedbacks in CMIP6 models and
433 their comparison to CMIP5 models, *Biogeosciences*, 17, 4173-4222, 10.5194/bg-17-
434 4173-2020, 2020.
- 435 5. Bartlett, M. K., Detto, M., and Pacala, S. W.: Predicting shifts in the functional
436 composition of tropical forests under increased drought and CO₂ from trade-offs among
437 plant hydraulic traits, *Ecol Lett*, 22, 67-77, 10.1111/ele.13168, 2019.
- 438 6. Bartlett, M. K., Scoffoni, C., and Sack, L.: The determinants of leaf turgor loss point and
439 prediction of drought tolerance of species and biomes: a global meta-analysis, *Ecol Lett*,
440 15, 393-405, 10.1111/j.1461-0248.2012.01751.x, 2012.
- 441 7. Bartlett, M. K., Klein, T., Jansen, S., Choat, B., and Sack, L.: The correlations and
442 sequence of plant stomatal, hydraulic, and wilting responses to drought, *P Natl Acad Sci*
443 *USA*, 113, 13098-13103, 10.1073/pnas.1604088113, 2016.
- 444 8. Bartlett, M. K., Zhang, Y., Kreidler, N., Sun, S. W., Ardy, R., Cao, K. F., and Sack, L.:
445 Global analysis of plasticity in turgor loss point, a key drought tolerance trait, *Ecol Lett*,
446 17, 1580-1590, 10.1111/ele.12374, 2014.
- 447 9. Berenguer, E., Lennox, G. D., Ferreira, J., Malhi, Y., Aragao, L. E. O. C., Barreto, J. R.,
448 Espirito-Santo, F. D., Figueiredo, A. E. S., Franca, F., Gardner, T. A., Joly, C. A.,
449 Palmeira, A. F., Quesada, C. A., Rossi, L. C., de Seixas, M. M. M., Smith, C. C., Withey,



- 450 K., and Barlow, J.: Tracking the impacts of El Nino drought and fire in human-modified
451 Amazonian forests, *P Natl Acad Sci USA*, 118, ARTN e2019377118:
452 10.1073/pnas.2019377118, 2021.
- 453 10. Binks, O., Meir, P., Rowland, L., da Costa, A. C. L., Vasconcelos, S. S., de Oliveira, A.
454 A. R., Ferreira, L., Christoffersen, B., Nardini, A., and Mencuccini, M.: Plasticity in leaf-
455 level water relations of tropical rainforest trees in response to experimental drought, *New*
456 *Phytol*, 211, 477-488, 10.1111/nph.13927, 2016.
- 457 11. Bonal, D., Burban, B., Stahl, C., Wagner, F., and Hérault, B.: The response of tropical
458 rainforests to drought-lessons from recent research and future prospects, *Ann Forest Sci*,
459 73, 27-44, 10.1007/s13595-015-0522-5, 2016.
- 460 12. Bonan, G. B.: Forests and climate change: Forcings, feedbacks, and the climate benefits
461 of forests, *Science*, 320, 1444-1449, 10.1126/science.1155121, 2008.
- 462 13. Boyle, B., Hopkins, N., Lu, Z., Raygoza Garay, J. A., Mozzherin, D., Rees, T., Matasci,
463 N., Narro, M. L., Piel, W. H., and McKay, S. J.: The taxonomic name resolution service:
464 an online tool for automated standardization of plant names, *BMC bioinformatics*, 14, 1-
465 15, 2013.
- 466 14. Breshears, D. D., Myers, O. B., Meyer, C. W., Barnes, F. J., Zou, C. B., Allen, C. D.,
467 McDowell, N. G., and Pockman, W. T.: Tree die-off in response to global change-type
468 drought: mortality insights from a decade of plant water potential measurements, *Front*
469 *Ecol Environ*, 7, 185-189, 10.1890/080016, 2009.
- 470 15. Caldwell, P. M., Mametjanov, A., Tang, Q., Van Roekel, L. P., Golaz, J. C., Lin, W. Y.,
471 Bader, D. C., Keen, N. D., Feng, Y., Jacob, R., Maltrud, M. E., Roberts, A. F., Taylor, M.
472 A., Veneziani, M., Wang, H. L., Wolfe, J. D., Balaguru, K., Cameron-Smith, P., Dong,
473 L., Klein, S. A., Leung, L. R., Li, H. Y., Li, Q., Liu, X. H., Neale, R. B., Pinheiro, M.,
474 Qian, Y., Ullrich, P. A., Xie, S. C., Yang, Y., Zhang, Y. Y., Zhang, K., and Zhou, T.: The
475 DOE E3SM Coupled Model Version 1: Description and Results at High Resolution, *J*
476 *Adv Model Earth Sy*, 11, 4095-4146, 10.1029/2019ms001870, 2019.
- 477 16. Chen, J. W., Zhang, Q., Li, X. S., and Cao, K. F.: Independence of stem and leaf
478 hydraulic traits in six Euphorbiaceae tree species with contrasting leaf phenology, *Planta*,
479 230, 459-468, 10.1007/s00425-009-0959-6, 2009.
- 480 17. Chitra-Tarak, R., Xu, C. G., Aguilar, S., Anderson-Teixeira, K. J., Chambers, J., Detto,
481 M., Faybishenko, B., Fisher, R. A., Knox, R. G., Koven, C. D., Kueppers, L. M., Kunert,
482 N., Kupers, S. J., McDowell, N. G., Newman, B. D., Paton, S. R., Perez, R., Ruiz, L.,
483 Sack, L., Warren, J. M., Wolfe, B. T., Wright, C., Wright, S. J., Zailaa, J., and McMahon,
484 S. M.: Hydraulically-vulnerable trees survive on deep-water access during droughts in a
485 tropical forest, *New Phytol*, 231, 1798-1813, 10.1111/nph.17464, 2021.
- 486 18. Choat, B., Jansen, S., Brodribb, T. J., Cochard, H., Delzon, S., Bhaskar, R., Bucci, S. J.,
487 Feild, T. S., Gleason, S. M., Hacke, U. G., Jacobsen, A. L., Lens, F., Maherali, H.,
488 Martinez-Vilalta, J., Mayr, S., Mencuccini, M., Mitchell, P. J., Nardini, A., Pittermann,
489 J., Pratt, R. B., Sperry, J. S., Westoby, M., Wright, I. J., and Zanne, A. E.: Global
490 convergence in the vulnerability of forests to drought, *Nature*, 491, 752-+,
491 10.1038/nature11688, 2012.
- 492 19. Christoffersen, B. O., Gloor, M., Fauset, S., Fyllas, N. M., Galbraith, D. R., Baker, T. R.,
493 Kruijt, B., Rowland, L., Fisher, R. A., Binks, O. J., Sevanto, S., Xu, C. G., Jansen, S.,
494 Choat, B., Mencuccini, M., McDowell, N. G., and Meir, P.: Linking hydraulic traits to



- 495 tropical forest function in a size-structured and trait-driven model (TFS v.1-Hydro),
496 Geosci Model Dev, 9, 4227-4255, 10.5194/gmd-9-4227-2016, 2016.
- 497 20. Fisher, R., McDowell, N., Purves, D., Moorcroft, P., Sitch, S., Cox, P., Huntingford, C.,
498 Meir, P., and Woodward, F. I.: Assessing uncertainties in a second-generation dynamic
499 vegetation model caused by ecological scale limitations, *New Phytol*, 187, 666-681,
500 10.1111/j.1469-8137.2010.03340.x, 2010.
- 501 21. Fisher, R. A. and Koven, C. D.: Perspectives on the Future of Land Surface Models and
502 the Challenges of Representing Complex Terrestrial Systems, *J Adv Model Earth Sy*, 12,
503 ARTN e2018MS001453: 10.1029/2018MS001453, 2020.
- 504 22. Fisher, R. A., Muszala, S., Versteinstein, M., Lawrence, P., Xu, C., McDowell, N. G.,
505 Knox, R. G., Koven, C., Holm, J., Rogers, B. M., Spessa, A., Lawrence, D., and Bonan,
506 G.: Taking off the training wheels: the properties of a dynamic vegetation model without
507 climate envelopes, *CLM4.5(ED)*, *Geosci Model Dev*, 8, 3593-3619, 10.5194/gmd-8-
508 3593-2015, 2015.
- 509 23. Fisher, R. A., Koven, C. D., Anderegg, W. R. L., Christoffersen, B. O., Dietze, M. C.,
510 Farrior, C. E., Holm, J. A., Hurtt, G. C., Knox, R. G., Lawrence, P. J., Lichstein, J. W.,
511 Longo, M., Matheny, A. M., Medvigy, D., Muller-Landau, H. C., Powell, T. L., Serbin,
512 S. P., Sato, H., Shuman, J. K., Smith, B., Trugman, A. T., Viskari, T., Verbeeck, H.,
513 Weng, E. S., Xu, C. G., Xu, X. T., Zhang, T., and Moorcroft, P. R.: Vegetation
514 demographics in Earth System Models: A review of progress and priorities, *Global
515 Change Biol*, 24, 35-54, 10.1111/gcb.13910, 2018.
- 516 24. Gleason, S. M., Westoby, M., Jansen, S., Choat, B., Hacke, U. G., Pratt, R. B., Bhaskar,
517 R., Brodrribb, T. J., Bucci, S. J., Cao, K. F., Cochard, H., Delzon, S., Domec, J. C., Fan,
518 Z. X., Feild, T. S., Jacobsen, A. L., Johnson, D. M., Lens, F., Maherali, H., Martinez-
519 Vilalta, J., Mayr, S., McCulloh, K. A., Mencuccini, M., Mitchell, P. J., Morris, H.,
520 Nardini, A., Pittermann, J., Plavcova, L., Schreiber, S. G., Sperry, J. S., Wright, I. J., and
521 Zanne, A. E.: Weak tradeoff between xylem safety and xylem-specific hydraulic
522 efficiency across the world's woody plant species, *New Phytol*, 209, 123-136,
523 10.1111/nph.13646, 2016.
- 524 25. Hochberg, U., Rockwell, F. E., Holbrook, N. M., and Cochard, H.: Iso/Anisohydry: A
525 Plant-Environment Interaction Rather Than a Simple Hydraulic Trait, *Trends Plant Sci*,
526 23, 112-120, 10.1016/j.tplants.2017.11.002, 2018.
- 527 26. Huang, M. Y., Xu, Y., Longo, M., Keller, M., Knox, R. G., Koven, C. D., and Fisher, R.
528 A.: Assessing impacts of selective logging on water, energy, and carbon budgets and
529 ecosystem dynamics in Amazon forests using the Functionally Assembled Terrestrial
530 Ecosystem Simulator, *Biogeosciences*, 17, 4999-5023, 10.5194/bg-17-4999-2020, 2020.
- 531 27. Iversen, C. M., McCormack, M. L., Powell, A. S., Blackwood, C. B., Freschet, G. T.,
532 Kattge, J., Roumet, C., Stover, D. B., Soudzilovskaia, N. A., Valverde-Barrantes, O. J.,
533 van Bodegom, P. M., and Violle, C.: A global Fine-Root Ecology Database to address
534 below-ground challenges in plant ecology, *New Phytol*, 215, 15-26, 10.1111/nph.14486,
535 2017.
- 536 28. Kennedy, D., Swenson, S., Oleson, K. W., Lawrence, D. M., Fisher, R., da Costa, A. C.
537 L., and Gentine, P.: Implementing Plant Hydraulics in the Community Land Model,
538 Version 5, *J Adv Model Earth Sy*, 11, 485-513, 10.1029/2018ms001500, 2019.



- 539 29. Klein, T.: The variability of stomatal sensitivity to leaf water potential across tree species
540 indicates a continuum between isohydric and anisohydric behaviours, *Funct Ecol*, 28,
541 1313-1320, 10.1111/1365-2435.12289, 2014.
- 542 30. Koven, C. D., Knox, R. G., Fisher, R. A., Chambers, J. Q., Christoffersen, B. O., Davies,
543 S. J., Detto, M., Dietze, M. C., Faybishenko, B., Holm, J., Huang, M. Y., Kovenock, M.,
544 Kueppers, L. M., Lemieux, G., Massoud, E., McDowell, N. G., Muller-Landau, H. C.,
545 Needham, J. F., Norby, R. J., Powell, T., Rogers, A., Serbin, S. P., Shuman, J. K., Swann,
546 A. L. S., Varadharajan, C., Walker, A. P., Wright, S. J., and Xu, C. G.: Benchmarking
547 and parameter sensitivity of physiological and vegetation dynamics using the
548 Functionally Assembled Terrestrial Ecosystem Simulator (FATES) at Barro Colorado
549 Island, Panama, *Biogeosciences*, 17, 3017-3044, 10.5194/bg-17-3017-2020, 2020.
- 550 31. Kunert, N., Zailaa, J., Herrmann, V., Muller-Landau, H. C., Wright, S. J., Perez, R.,
551 McMahon, S. M., Condit, R. C., Hubbell, S. P., Sack, L., Davies, S. J., and Anderson-
552 Teixeira, K. J.: Leaf turgor loss point shapes local and regional distributions of evergreen
553 but not deciduous tropical trees, *New Phytol*, 230, 485-496, 10.1111/nph.17187, 2021.
- 554 32. Kursar, T. A., Engelbrecht, B. M. J., Burke, A., Tyree, M. T., El Omari, B., and Giraldo,
555 J. P.: Tolerance to low leaf water status of tropical tree seedlings is related to drought
556 performance and distribution, *Funct Ecol*, 23, 93-102, 10.1111/j.1365-
557 2435.2008.01483.x, 2009.
- 558 33. Manzoni, S., Vico, G., Katul, G., Palmroth, S., Jackson, R. B., and Porporato, A.:
559 Hydraulic limits on maximum plant transpiration and the emergence of the safety-
560 efficiency trade-off, *New Phytol*, 198, 169-178, 10.1111/nph.12126, 2013.
- 561 34. Massoud, E. C., Xu, C. G., Fisher, R. A., Knox, R. G., Walker, A. P., Serbin, S. P.,
562 Christoffersen, B. O., Holm, J. A., Kueppers, L. M., Ricciuto, D. M., Wei, L., Johnson,
563 D. J., Chambers, J. Q., Koven, C. D., McDowell, N. G., and Vrugt, J. A.: Identification of
564 key parameters controlling demographically structured vegetation dynamics in a land
565 surface model: CLM4.5(FATES), *Geosci Model Dev*, 12, 4133-4164, 10.5194/gmd-12-
566 4133-2019, 2019.
- 567 35. McDowell, N., Allen, C. D., Anderson-Teixeira, K., Brando, P., Brien, R., Chambers,
568 J., Christoffersen, B., Davies, S., Doughty, C., Duque, A., Espirito-Santo, F., Fisher, R.,
569 Fontes, C. G., Galbraith, D., Goodsman, D., Grossiord, C., Hartmann, H., Holm, J.,
570 Johnson, D. J., Kassim, A., Keller, M., Koven, C., Kueppers, L., Kumagai, T., Malhi, Y.,
571 McMahon, S. M., Mencuccini, M., Meir, P., Moorcroft, P., Muller-Landau, H. C.,
572 Phillips, O. L., Powell, T., Sierra, C. A., Sperry, J., Warren, J., Xu, C. G., and Xu, X. T.:
573 Drivers and mechanisms of tree mortality in moist tropical forests, *New Phytol*, 219, 851-
574 869, 10.1111/nph.15027, 2018.
- 575 36. McDowell, N. G., Sapes, G., Pivovarov, A., Adams, H. D., Allen, C. D., Anderegg, W.
576 R. L., Arend, M., Breshears, D. D., Brodrick, T., Choat, B., Cochard, H., De Caceres, M.,
577 De Kauwe, M. G., Grossiord, C., Hammond, W. M., Hartmann, H., Hoch, G., Kahmen,
578 A., Klein, T., Mackay, D. S., Mantova, M., Martinez-Vilalta, J., Medlyn, B. E.,
579 Mencuccini, M., Nardini, A., Oliveira, R. S., Sala, A., Tissue, D. T., Torres-Ruiz, J. M.,
580 Trowbridge, A. M., Trugman, A. T., Wiley, E., and Xu, C. G.: Mechanisms of woody-
581 plant mortality under rising drought, CO₂ and vapour pressure deficit, *Nat Rev Earth
582 Env*, 3, 294-308, 10.1038/s43017-022-00272-1, 2022.



- 583 37. Moorcroft, P. R., Hurtt, G. C., and Pacala, S. W.: A method for scaling vegetation
584 dynamics: The ecosystem demography model (ED), *Ecol Monogr*, 71, 557-585,
585 10.1890/0012-9615(2001)071[0557:Amfsvd]2.0.Co;2, 2001.
- 586 38. Needham, J. F., Chambers, J., Fisher, R., Knox, R., and Koven, C. D.: Forest responses to
587 simulated elevated CO₂ under alternate hypotheses of size- and age-dependent mortality,
588 *Global Change Biol*, 26, 5734-5753, 10.1111/gcb.15254, 2020.
- 589 39. Paton, S.: Yearly Reports Barro Colorado Island, Smithsonian Tropical Research
590 Institute, <https://doi.org/10.25573/data.11799111.v3>, 2020.
- 591 40. Pineda-Garcia, F., Paz, H., and Meinzer, F. C.: Drought resistance in early and late
592 secondary successional species from a tropical dry forest: the interplay between xylem
593 resistance to embolism, sapwood water storage and leaf shedding, *Plant Cell Environ*, 36,
594 405-418, 10.1111/j.1365-3040.2012.02582.x, 2013.
- 595 41. Powell, T. L., Wheeler, J. K., de Oliveira, A. A. R., da Costa, A. C. L., Saleska, S. R.,
596 Meir, P., and Moorcroft, P. R.: Differences in xylem and leaf hydraulic traits explain
597 differences in drought tolerance among mature Amazon rainforest trees, *Global Change*
598 *Biol*, 23, 4280-4293, 10.1111/gcb.13731, 2017.
- 599 42. Powell, T. L., Koven, C. D., Johnson, D. J., Faybishenko, B., Fisher, R. A., Knox, R. G.,
600 McDowell, N. G., Condit, R., Hubbell, S. P., Wright, S. J., Chambers, J. Q., and
601 Kueppers, L. M.: Variation in hydroclimate sustains tropical forest biomass and promotes
602 functional diversity, *New Phytol*, 219, 932-946, 10.1111/nph.15271, 2018.
- 603 43. Roderick, M. L., Berry, S. L., Saunders, A. R., and Noble, I. R.: On the relationship
604 between the composition, morphology and function of leaves, *Funct Ecol*, 13, 696-710,
605 DOI 10.1046/j.1365-2435.1999.00369.x, 1999.
- 606 44. Rowland, L., da Costa, A. C. L., Galbraith, D. R., Oliveira, R. S., Binks, O. J., Oliveira,
607 A. A. R., Pullen, A. M., Doughty, C. E., Metcalfe, D. B., Vasconcelos, S. S., Ferreira, L.
608 V., Malhi, Y., Grace, J., Mencuccini, M., and Meir, P.: Death from drought in tropical
609 forests is triggered by hydraulics not carbon starvation, *Nature*, 528, 119+,
610 10.1038/nature15539, 2015.
- 611 45. Sack, L., Cowan, P. D., Jaikumar, N., and Holbrook, N. M.: The 'hydrology' of leaves:
612 co-ordination of structure and function in temperate woody species, *Plant Cell Environ*,
613 26, 1343-1356, DOI 10.1046/j.0016-8025.2003.01058.x, 2003.
- 614 46. Savage, V. M., Bentley, L. P., Enquist, B. J., Sperry, J. S., Smith, D. D., Reich, P. B., and
615 von Allmen, E. I.: Hydraulic trade-offs and space filling enable better predictions of
616 vascular structure and function in plants, *P Natl Acad Sci USA*, 107, 22722-22727,
617 10.1073/pnas.1012194108, 2010.
- 618 47. Sperry, J. S. and Love, D. M.: What plant hydraulics can tell us about responses to
619 climate-change droughts, *New Phytol*, 207, 14-27, 10.1111/nph.13354, 2015.
- 620 48. Su, R., Liu, H., Wang, C., Zhang, H., and Cui, J.: Leaf turgor loss point is one of the best
621 predictors of drought-induced tree mortality in tropical forest, *Front Ecol Evol*, 10,
622 ARTN 974004: 10.3389/fevo.2022.974004, 2022.
- 623 49. Wolfe, B. T.: Bark water vapour conductance is associated with drought performance in
624 tropical trees, *Biol Letters*, 16, ARTN 20200263: 10.1098/rsbl.2020.0263, 2020.
- 625 50. Wright, S. J., Kitajima, K., Kraft, N. J. B., Reich, P. B., Wright, I. J., Bunker, D. E.,
626 Condit, R., Dalling, J. W., Davies, S. J., Diaz, S., Engelbrecht, B. M. J., Harms, K. E.,
627 Hubbell, S. P., Marks, C. O., Ruiz-Jaen, M. C., Salvador, C. M., and Zanne, A. E.:



- 628 Functional traits and the growth-mortality trade-off in tropical trees, *Ecology*, 91, 3664-
629 3674, Doi 10.1890/09-2335.1, 2010.
- 630 51. Xu, C. G. and Gertner, G.: Understanding and comparisons of different sampling
631 approaches for the Fourier Amplitudes Sensitivity Test (FAST), *Comput Stat Data An*,
632 55, 184-198, 10.1016/j.csda.2010.06.028, 2011a.
- 633 52. Xu, C. G. and Gertner, G. Z.: Reliability of global sensitivity indices, *J Stat Comput Sim*,
634 81, 1939-1969, 10.1080/00949655.2010.509317, 2011b.
- 635 53. Xu, C. G., McDowell, N. G., Fisher, R. A., Wei, L., Sevanto, S., Christoffersen, B. O.,
636 Weng, E. S., and Middleton, R. S.: Increasing impacts of extreme droughts on vegetation
637 productivity under climate change, *Nat Clim Change*, 9, 948+, 10.1038/s41558-019-
638 0630-6, 2019.
- 639 54. Xu, X. T., Medvigy, D., Powers, J. S., Becknell, J. M., and Guan, K. Y.: Diversity in
640 plant hydraulic traits explains seasonal and inter-annual variations of vegetation
641 dynamics in seasonally dry tropical forests, *New Phytol*, 212, 80-95, 10.1111/nph.14009,
642 2016.
- 643 55. Yang, S. D. and Tyree, M. T.: Hydraulic Resistance in *Acer-Saccharum* Shoots and Its
644 Influence on Leaf Water Potential and Transpiration, *Tree Physiol*, 12, 231-242, DOI
645 10.1093/treephys/12.3.231, 1993.
- 646